Early differentiation processes on Mars inferred from silicon isotopes

Delphine Losno, Caroline Fitoussi, Bernard Bourdon

Geochimica et Cosmochimica Acta 338 (2022) 11–23

Contents lists available at ScienceDirect

Geochimica et Cosmochimica Acta

journal homepage: www.elsevier.com/locate/gca

Early differentiation processes on Mars inferred from silicon isotopes

Delphine Losno, Caroline Fitoussi, Bernard Bourdon *

Laboratoire de Géologie de Lyon, Terre, Planètes, Environnement, ENS de Lyon, UCBL, CNRS, 46 Allée d'Italie, 69364 Lyon cedex 07, France

ARTICLE INFO

Article history:
Received 4 April 2022
Accepted 3 October 2022
Available online 10 October 2022
Associate editor: Helen Williams

Keywords:
Mars
Magma ocean
Silicon isotope
Isotope fractionation

ABSTRACT

Accretion of terrestrial planets involved partial or global melting events such as magma oceans or magma ponds. Mars experienced large-scale differentiation very early in its history, as shown by its ^{146}Sm-^{142}Nd and ^{182}Hf-^{182}W record. The broad variations in ε^{142}Nd and ε^{142}W of SNC meteorites highlight the presence of mantle sources that must have remained isolated, at least partly, after the crystallization of a global magma ocean. In this study, we have investigated whether the crystallization of the martian magma ocean could have generated mantle reservoirs characterized by different silicon isotope signatures, as the fractionation of Si isotopes between minerals and melts is known to depend on pressure. Thus, the goal of this study was to investigate whether there were any relationships between magma ocean crystallisation and possible variations in the Si isotope record of SNC meteorites. High resolution silicon isotope measurements were performed on twelve meteorites from the Shergottite, Nakhlite and Chassignite groups using a Neptune Plus MC-ICP-MS in dry plasma mode. The δ^{30}Si values are in good agreement with previous studies but display a narrower range of variations with a mean value at −0.46 ‰ ± 0.07 (2SD). A magma ocean crystallization model shows that the range of δ^{30}Si in SNCs is consistent with that generated by magma ocean crystallisation. In particular, there is a correlation between calculated ^{147}Sm/^{144}Nd for the moderately depleted mantle sources with δ^{30}Si values; this correlation is consistent with the crystallization model if one includes trapped melt in the cumulates. In contrast, enriched shergottites displayed a very homogenous composition in Sm/Nd ratios, despite significant variability in δ^{30}Si. This observation could be related to either fluid-rock interactions or redox effect during magma differentiation. Altogether, silicon isotope compositions of SNC provide new constraints about magma ocean crystallization processes in Mars.

1. Introduction

The isotope composition of major elements such as Fe, Mg and Si in planetary materials has been the focus of various studies aiming at better understanding accretion and differentiation processes leading to the chemical diversity among planetary bodies (e.g. Dauphas et al., 2015; Fitoussi et al., 2009; Hin et al., 2017; Magna et al., 2017; Sossi et al., 2016; Williams et al., 2021). The Earth, Moon, Mars and smaller objects of the inner Solar System likely experienced a partially or totally molten state following their accretion (Solomatov, 2000, 2007; Reese and Solomatov, 2006; Elkins-Tanton, 2012; Schaefer and Elkins-Tanton, 2018). The sources of energy to produce such a magma ocean are linked with accretion processes, core formation and radioactive decay of short-lived radioisotope such as ^{26}Al, provided the accretion timescale was sufficiently rapid (half-life of 0.717 Myr) (Elkins-Tanton, 2012). The large amount of energy released by impacts during accretion and differentiation was sufficient to entirely melt a Mars-size object (Elkins-Tanton, 2005; Nimmo and Kleine, 2007; Plesa et al., 2014). The complete separation of metal and silicate during core formation of the Earth and Mars should also yield complete mantle melting, thereby allowing metallic liquid percolation throughout the entire mantle (Terasaki et al., 2005).

The SNC meteorites (Shergottite, Nahklite and Chassignite group) are basaltic to ultramafic rocks that are thought to have been ejected from the surface of Mars (McSween, 1994; Treiman et al., 2000). The shergottites show a large variation in ε^{142}Nd and ε^{142}W indicating heterogeneous mantle sources that were formed when the parent isotopes of ^{142}Nd and ^{182}W were still extant (Harper et al., 1995; Foley et al., 2005; Debaille et al., 2007; Caro et al., 2008; Kruijer et al., 2017). Thus, mantle differentiation must have occurred very early in Mars history and the time scale of differentiation was estimated to range between 20 Myr after the beginning of the Solar System (Bouvier et al., 2018; Kruijer et al., 2020) and 100 Myr in the case of a protracted magma

* Corresponding author.
E-mail address: bernard.bourdon@ens-lyon.fr (B. Bourdon).

https://doi.org/10.1016/j.gca.2022.10.002
0016-7037/

ocean (Debaille et al., 2007; Caro et al., 2008; Borg et al., 2016; Kruijer et al., 2017). Subsequently, the geochemical evolution of SNC mantle sources has been explained by various models highlighting a complex magmatic history (Blichert-Toft et al., 1999; Jones, 2003; Papike et al., 2009; McCubbin et al., 2013).

The preservation of ^{142}Nd and ^{182}W anomalies in SNC shows evidence for inefficient mantle mixing following magma ocean crystallization and is corroborated by dynamical models of mantle evolution (e.g. Breuer and Spohn, 2003; Kiefer 2003). The study of Huang et al. (2014) has shown that in the Earth, magma ocean crystallization could impart a Si isotope signature typical of the lower mantle that would be distinct from the upper mantle. The crystallization of a magma ocean (Draper et al., 2003; Draper et al., 2005; Elkins-Tanton et al., 2003; Bertka and Fei, 1997) should in principle involve at least the presence of majorite and ringwoodite or even perhaps bridgmanite (Mg-perovskite), which have been shown to involve a larger Si isotope fractionation factor compared with other minerals (Huang et al., 2014). Note, however, that in principle according to recent models for Mars composition (e.g. Yoshizaki and McDonough 20), bridgmanite should not be present in the martian mantle). Thus, the fractional crystallization of the MMO (Martian Magma Ocean) could potentially give rise to the presence of different Si isotope reservoirs. Given that the Mars mantle shows a better preservation of old magma-ocean related signatures in other isotope systems, one could imagine that it is worth investigating Si isotopes from that perspective.

In this respect, the silicon isotope signatures of SNC could also reflect the composition of their various mantle sources, as magmatic melting and differentiation does not greatly fractionate silicon isotopes, provided the SiO_2 contents are below 55 wt% (Fitoussi et al., 2009; Savage et al., 2014). It has been suggested that evaporation processes from the surface of the magma ocean could have fractionated silicon isotopes in the case of the Earth (Hin et al., 2017). Thus, one could argue that similar processes could have operated since Mars also experienced a magma ocean stage. In contrast, a recent study by Tang and Young (2020) indicates no significant Si mass-dependent fractionation is likely to take place while a planet-size body had a magma ocean. It was also shown by Dauphas et al. (2015) that impact-induced Si volatilization was also not likely to have induced silicon isotope fractionation on Moon and Mars sized planetesimals. In addition, one also needs to take into account the potential effect of core formation, as this process has been shown to affect the Si isotope composition of planetary mantles (e.g., Bourdon et al., 2018).

Previous studies of Si isotopes in SNC meteorites have shown a large range in δ^{30}Si values (–0.33 to −0.61 ‰) and this could be indicative of analytical biases between laboratories (Armytage et al., 2011; Pringle et al., 2013; Zambardi et al., 2013) or of a true isotope heterogeneity, although it is difficult to conclude as these studies had few samples in common.

In this study, we revisited this issue by analyzing a larger collection of martian meteorites using a Neptune Plus MC-ICP-MS operating in dry plasma mode. These new Si isotope measurements define a precise dataset of silicon isotope signature for the different martian mantle sources and this data set is used to investigate whether magma ocean signatures could still be present in the martian mantle.

2. Sample preparation and analytical methods

2.1. Sample description

Samples analysed in this study include ten martian meteorites which belong to the shergottite group (LAR06319, LAR12011, RBT04262, NWA856, NWA480, EET790010-A and B, Zagami and NWA), one meteorite from the nakhlite group (MIL03346) and one from the chassignite group (NWA2737) (see Supplementary Materials, Tables S1 and S2). The three different groups share similar oxygen isotope composition expressed as Δ^{17}O (Clayton and Mayeda, 1983) and show homogeneous redox state *within* each group (Stolper et al., 1979; Wadhwa, 2001; Herd, 2003) although a recent study argues for a homogeneous f_{O2} in the martian mantle (Nicklas et al., 2021). The relatively young crystallization age of shergottites, between 170 and 341 Ma (see compilation by McSween and McLennan, 2014) compared with other extra-terrestrial materials means that the formation of SNC are associated with relatively recent igneous processes that could be related to Mars mantle-crust evolution (Bogard and Johnson, 1983; Udry et al., 2014; Filiberto, 2017; Day et al., 2018; Mezger et al. Udry et al., 2020). The SNC meteorites consist of mafic and ultramafic cumulate rocks with various magmatic history (McSween, 1994; Udry et al., 2020). The classification of SNC is based on their incompatible trace element relative enrichment and three groups can be distinguished, depleted, intermediate and enriched, corresponding to various levels in the La/Yb ratio (e.g. Udry et al., 2020). In parallel, the shergottite group is also divided according to their petrological type (Udry et al., 2020) and this classification was followed in Table 3 and Tables S1 and S2. The basaltic shergottites have basaltic textures with major mineral phases consisting of clinopyroxenes (pigeonite and augite) and plagioclase (in the form of glass or maskelynite produced by shocks). Poikilitic shergottites present a poikilitic texture consisting mainly of olivine with clinopyroxene and orthopyroxene. The olivine-phyric group presents olivine porphyritic texture, low augite content and chromite in addition to other minor mineral phases. Nakhlite MIL03346 consisting mainly of clinopyroxene was classified as a clinopyroxenite and Chassignite NWA2737 composed essentially of olivine was classified as a dunite. The nakhlite and chassignite group share similar crystallization ages, ejection ages and trace element compositions that suggested a common magmatic petrogenesis (Jones, 1989; McCubbin et al., 2013). The twelve analyzed samples were not exposed to significant terrestrial or martian weathering and presented shock features as melt pockets (see Supplementary Materials, Table S2).

2.2. Sample preparation

The samples were first cleaned in an ultrasonic bath with deionized water followed by a bath in distilled ethanol. Samples were then powdered in an agate mortar that was pre-cleaned with 0.5 M HNO_3. The primary standard reference material SRM 8546 (consisting of ultra-pure silica powder), secondary standards Diatomite and BHVO-2 and martian samples were dissolved using an alkali fusion method adapted from the procedure described in Georg et al. (2006). Between 1 and 4 mg of powdered sample was melted at 730 °C in a silver crucible with a ≈ 200 mg NaOH pellet for 7 min and 30 s. After letting the fusion cake cool down, the crucible was transferred to a 30 ml Savillex vial filled with Milli-Q Element water. An ultrasonic tip was introduced in the vial for 4 min and the solution was left to equilibrate at 120° on a hotplate overnight. The solutions were then transferred to Teflon bottles and the vials were rinsed with Milli-Q water until the silicon concentration was diluted to 6 ppm. A solution of 6 M HCl was then added to reach a pH between 2 and 3 which is a necessary condition for reliable silicon isotope analysis (Fitoussi et al., 2009).

2.3. Column chromatography

A solution corresponding to approximately 3 μg of silicon was loaded on a BioRad column filled with 1 ml of cation exchange resin BioRad 50 W-X8, 200–400 mesh in H^+ form. The separation

procedure was adapted from the initial procedure described by Georg et al. (2006) and the new separation protocol is summarized in Table 1. The cations stick to the resin whereas the silicic acid (H_4SiO_4 and $H_3SiO_4^-$ in acidic water solution) goes through the column and thus the Si fraction is collected with a yield close to 100 %.

2.4. Mass spectrometry

Silicon isotopic measurements were performed on a Neptune Plus MC-ICP-MS in dry plasma mode using a DSN-100 desolvating nebulizer introduction system. The aerosol was introduced in the plasma by a silicon torch equipped with a sapphire injector to minimize Si instrumental blank. The mass spectrometer was run in medium resolution mode with a resolving power of ≈ 7500 which allows to resolve silicon isotope ion beams from polyatomic interferences on the high mass side of the peak plateau (e.g. $^{12}C^{16}O^+$ and $^{14}N_2$ on $^{28}Si^+$; $^{12}C^{17}O^+$, $^{14}N^{15}N^+$, $^{12}C^{17}O^+$ on $^{29}Si^+$; $^{12}C^{18}O^+$, $^{14}N^{16}O^+$ on $^{30}Si^+$). The measuring position for 28, 29 and 30 amu on the peak shoulder is illustrated in Fig. S1 that also shows the level of interferences. All instrumental parameters were optimized to reach maximum sensitivity, signal stability and signal to noise ratio and the running conditions are given in Table 2. The signal to noise ratio was increased by modifying the nature of the injector (sapphire versus quartz) as well as the running parameters (e.g. position of the torch, RF power). This overall increased the signal to noise ratio by a factor of at least 10. The instrumental mass fractionation was corrected by the sample-standard bracketing method. Silicon isotope compositions are expressed in per mil variation relative to the NBS-28 standard using the following equation with exponent x corresponding to either 29 or 30:

$$\delta^x Si = \left[\frac{\left(\frac{\delta^x Si}{\delta^{28} Si}\right)_{sample}}{\left(\frac{\delta^x Si}{\delta^{28} Si}\right)_{NBS-28}} - 1 \right] \times 1000 \quad (1)$$

The electronic background level on the Faraday cup amplifiers was measured over 60 s and subtracted prior to each sample measurement. Each sample was measured over one block of 36 cycles with an integration time of 8.389 s, each amplifier being equipped with 10^{11} Ω resistors. An on-peak-zero (OPZ) correction was carried out by measuring the intensities of the three silicon masses in the cleanest 0.002 M HCl wash over 75 s before and after each analysis.

The Diatomite was used as a secondary standard at the beginning and within each measurement sequence to ensure the accuracy and mass dependence of the measurements. The well-characterized terrestrial Hawaiian basalt BHVO-2 was also used to assess the reproducibility of our measurements. The $\delta^{30}Si$ for these standards are 1.25 ± 0.16 ‰ (±2SD, N = 429) for the Diatomite and −0.27 ± 0.13 ‰ (±2SD, N = 131) for BHVO-2, which is in good agreement with literature data as summarized in Table 5.

Table 1
Column chromatography procedure for silicon separation.

Separation Stage	Solution	Volume
Pre-cleaning resin	3 N HCl	Column reservoir
Pre-cleaning resin	6 N HCl	Column reservoir
Pre-cleaning resin	15 N HNO_3	200 µl
Pre-cleaning resin	6 N HCl	Column reservoir
Pre-cleaning resin	3 N HCl	Column reservoir
Pre-cleaning resin	Milli-Q	4 column reservoirs
Sample load	Acidified sample solution to pH 2–3	≈ 0.5 ml
Elution	Milli-Q	2 ml
Dilution to running concentration	Milli-Q	Between 2 and 5 ml

Table 2
Instrumental settings for silicon isotope analysis on the Neptune Plus MC-ICP-MS.

Parameter	Neptune Plus
Rf power	1200
Sampler cone	Standard "H"-type, Nickel
Skimmer cone	Jet "X"-type, Nickel
Coolant gas (Ar) flow	16 l/min
Auxiliary gas (Ar) flow	1.23 l/min
Z torch position	2.5 mm
Nebulizer uptake rate	≈ 70 µl/min
Cup configuration	H3: ^{30}Si; C: ^{29}Si; L3: ^{28}Si
Si running concentration	0.5 ppm
Sensitivity on ^{28}Si beam	≈ 15 V
Instrumental blank	≈ 150 mV
Desolvating device	DSN-100
DSN nebulizer pressure	30 PSI
DSN hot gas flow	0.2 l/min
DSN membrane gas (Ar) flow	≈ 4–5 l/min

3. Results

The silicon isotope compositions for twelve martian meteorites, one lunar sample 70017 and the two secondary standards Diatomite and BHVO-2 are reported Table 3 and shown in Fig. 1 for checking consistency with previous work (e.g. Fitoussi and Bourdon 2012). All measured Si isotope data were mass dependent and this was used as a validity check. The three-isotope plot, $\delta^{29}Si$ versus $\delta^{30}Si$ yielded a slope of 0.5055 which is consistent with the slopes of equilibrium (0.5178) and kinetic (0.5092) isotope fractionation (Fig. 2b).

The lunar $\delta^{30}Si$ value of −0.33 ± 0.01 ‰ (2SE, N = 12) coincides with recent $\delta^{30}Si$ reported in the literature (Georg et al., 2007; Fitoussi and Bourdon, 2012; Armytage et al., 2012; Zambardi et al., 2013). The $\delta^{30}Si$ values of martian meteorites analyzed in this study range from −0.41 to −0.52 ‰ leading to a mean $\delta^{30}Si$ for SNC equal to −0.46 ± 0.07 ‰ (2SD), in agreement with previous studies (Table 4). Nevertheless, the spread in $\delta^{30}Si$ values of SNC is more limited than in previous studies. The $\delta^{30}Si$ of Nakhlite MIL03346 was previously measured by Zambardi et al. (2013) with a mean of −0.49 ± 0.06 ‰ (2SE) close to the value of −0.50 ± 0.02 ‰ (2SE) obtained in this study. The enriched shergottite Zagami was also measured by Zambardi et al. (2013) with a $\delta^{30}Si$ value of −0.49 ± 0.05 ‰ (2SE) and by Armytage et al. (2011) with a higher $\delta^{30}Si$ value equal to −0.39 ± 0.04 ‰ (2SE). The $\delta^{30}Si$ for Zagami obtained in this study (−0.46 ± 0.02) is closer to the value given by Zambardi et al. (2013) (−0.49 ± 0.05 ‰, 2SE). The $\delta^{30}Si$ values of the Nakhlite MIL03346 (−0.50 ± 0.02) and Chassignite NWA2737 (−0.52 ± 0.02) analyzed in this study indicate a slight enrichment in light isotopes compared with the mean of −0.45 ± 0.02 ‰ (2SE) of shergottites.

4. Discussion

4.1. Role of core formation on the Si isotope composition of SNC meteorites

Silicon partitioning experiments between metal and silicate have demonstrated that the metal fraction should be enriched in light Si isotopes, while an enrichment in heavy Si isotopes was found for the silicate phase (Shahar et al., 2009, 2011; Javoy et al., 2012; Hin et al., 2014). The silicon isotope composition of

Table 3
Silicon isotope data for martian meteorites.

	Nature	$\delta^{29}Si$	2SE	$\delta^{30}Si$	2SE	N[1]	SiO_2 (wt%)[2]
Standards							
Diatomite (±2SD)		0.64	0.09*	1.25	0.16*	429	100
BHVO-2	Hawaïan basalt	−0.14	0.01	−0.27	0.02	43	49.9
Moon							
70017	Ilmenite basalt	−0.16	0.01	−0.33	0.01	12	38.5
Martian Meteorites							
Depleted[3]							
DaG-476	Ol-phyric Shergottite	−0.20	0.03	−0.43	0.03	5	45.4
SaU-005	Ol-phyric Shergottite	−0.21	0.02	−0.45	0.02	5	46.3
Intermediate							
NWA480	Basaltic Shergottite	−0.22	0.01	−0.44	0.02	12	50.3
EET790010A	Ol-phyric Shergottite	−0.22	0.01	−0.44	0.03	10	51.7
EET790010B	Ol-phyric Shergottite	−0.25	0.01	−0.47	0.02	12	49.9
ALH77005	Poikilitic Shergottite	−0.22	0.01	−0.43	0.02	12	41.3
Enriched							
LAR06319	Ol-phyric Shergottite	−0.21	0.02	−0.42	0.05	8	46.7
LAR12011	Ol-phyric Shergottite	−0.25	0.02	−0.49	0.03	12	46.7
RBT04262	Poikilitic Shergottite	−0.25	0.02	−0.45	0.02	12	47.6
Zagami	Basaltic Shergottite	−0.23	0.01	−0.46	0.02	12	51.2
NWA856	Basaltic shergottite	−0.21	0.02	−0.41	0.05	8	48.9
NWA14017	Ol-phyric shergottite	−0.24	0.02	−0.47	0.04	18	_
NWA2737	Chassignite	−0.27	0.01	−0.52	0.02	17	37
MIL03346	Naklite, cpxnite	−0.26	0.01	−0.50	0.02	26	49.5
Mars average (±2SD)		−0.24	0.04	−0.46	0.07	N = 12	

[1] N is the number of measurements of each sample.
[2] Silicon concentrations are obtained from the Lunar Sample Compendium for 70017 and the Martian Meteorite Compendium for the SNC and from the United States Geological Survey for BHVO-2.
[3] Silicon isotope data of depleted shergottites are from Zambardi et al. (2013).
* ±2 S.D. (for the Diatomite only).

Table 4
Comparison of recent Si isotope data for martian meteorites.

Martian mean from	$\delta^{29}Si$	2SD	$\delta^{30}Si$	2SD	Number of samples
This study	−0.24	0.04	−0.46	0.07	N = 12
Pringle et al. (2013)	−0.24	0.04	−0.48	0.07	N = 6
Zambardi et al. (2013)	−0.22	0.08	−0.49	0.09	N = 9
Armytage et al. (2011)	−0.25	0.08	−0.48	0.13	N = 5

martian mantle rocks could thus have been shifted due to core formation processes. Temperature, pressure and oxygen fugacity (fO_2) conditions under which martian core formed have been established based on the abundances of siderophile elements in SNC (Righter and Drake, 1996; Righter and Chabot, 2011; Rai and van Westrenen, 2013; Yang et al., 2015). According to these studies, the conditions of Mars core formation were rather oxidizing conditions with a calculated ΔIW (fO_2 relative to the iron-wüstite buffer) of −1.25 at a temperature of ≈ 2400 K while the maximum pressure of metal segregation did not exceed 14 ± 3 GPa. This depth is shallower than the depth of the magma ocean (20 GPa) but this may be due to the fact that metal droplets near the boundary can be re-entrained by silicate convection, thereby yielding a lower depth of metal silicate equilibration (Righter and Chabot 2011). These redox conditions and the moderate pressure of core segregation prevented silicon from entering the metallic phase in substantial amounts (Kilburn and Wood, 1997; Gessmann et al., 2001; Steenstra et al., 2020). Silicon isotope compositions of SNC were thus not affected by core formation processes.

4.2. Si isotope fractionation during magmatic differentiation

The behavior of silicon isotopes during magmatic differentiation was reviewed by Savage et al. (2014) who showed a positive slope between silica content and $\delta^{30}Si$ for a suite of terrestrial rocks as already suggested by an older study of Douthitt (1982). As magmas get differentiated by fractional crystallization, the magma becomes more enriched in silica and in heavy isotopes.

When considering the effect of partial melting, there was no offset between mantle peridotites and the more mafic compositions (i.e. basalts), suggesting that the $\delta^{30}Si$ of basalts were representative of their mantle sources (Fitoussi et al., 2009; Armytage et al., 2011; Zambardi et al., 2013). The variations in Si isotopes of martian meteorites shows no correlation (R^2 = 0.14) with their silica or MgO contents (not shown) (Fig. 3). Hence, the Si isotope differences among the samples are not related to magmatic differentiation or partial melting. Unlike the terrestrial mantle which appears to be homogeneous with respect to Si isotopes (Fitoussi et al., 2009; Savage et al., 2014; Zambardi et al., 2013), the Martian mantle did not experience global mixing, as suggested by the large range in Nd and W isotope systematics (e.g. Foley et al., 2005; Debaille et al., 2007; Caro et al., 2008; Kruijer et al., 2017), such that the Si isotope variations among the SNC could be inherited from different mantle sources generated by the crystallization of the magma ocean.

4.3. Volatility-related Si isotope fractionation

The formation of a magma ocean could have led to Si isotope fractionation by evaporation, provided the existence of a liquid

Table 5
Silicon isotope composition of Diatomite and BHVO-2 standards from literature and from this study.

	$\delta^{30}Si$	2SD	$\delta^{29}Si$	2SD	N
Diatomite					
Reynolds et al. (2007)	1.26	0.2	0.64	0.14	82
Abraham et al. (2008)	1.25	0.14	0.64	0.1	24
Fitoussi et al. (2009)	1.24	0.19	0.64	0.09	89
Ziegler et al. (2010) [1]	1.22	0.18	0.63	0.008	1
Chakrabarti and Jacobsen (2010)	1.23	0.19	0.61	0.13	41
Savage et al. (2011)	1.23	0.1	0.64	0.08	177
Armytage et al. (2011)	1.23	0.15	0.63	0.1	400
Armytage et al. (2012)	1.23	0.14	0.63	0.09	250
Fitoussi and Bourdon (2012)	1.23	0.21	0.64	0.10	110
Savage and Moynier (2013)	1.22	0.1	0.63	0.06	43
This study	1.25	0.16	0.64	0.09	429
BHVO-2					
Abraham et al. (2008)	−0.29	0.31	−0.17	0.11	8
Fitoussi et al. (2009)	−0.32	0.15	−0.16	0.15	14
Savage et al. (2011)	−0.29	0.09	−0.15	0.08	188
Zambardi and Poitrasson (2011)	−0.27	0.08	−0.14	0.05	360
Armytage et al. (2011)	−0.30	0.09	−0.18	0.07	11
Armytage et al. (2012)	−0.28	0.14	−0.15	0.08	210
Zambardi et al. (2013)	−0.27	0.07	−0.14	0.04	54
Savage and Moynier (2013)	−0.28	0.09	−0.15	0.06	44
Pringle et al. (2013)	−0.28	0.12	−0.15	0.09	26
Pringle et al. (2014)	−0.31	0.12	−0.16	0.08	57
Dauphas et al. (2015) [2]	−0.262	0.053	−0.132	0.037	9
This study	−0.27	0.13	−0.14	0.07	131

[1] Error given as 2SE.
[2] Errors given as 95% intervals of the means of 9 analysis.

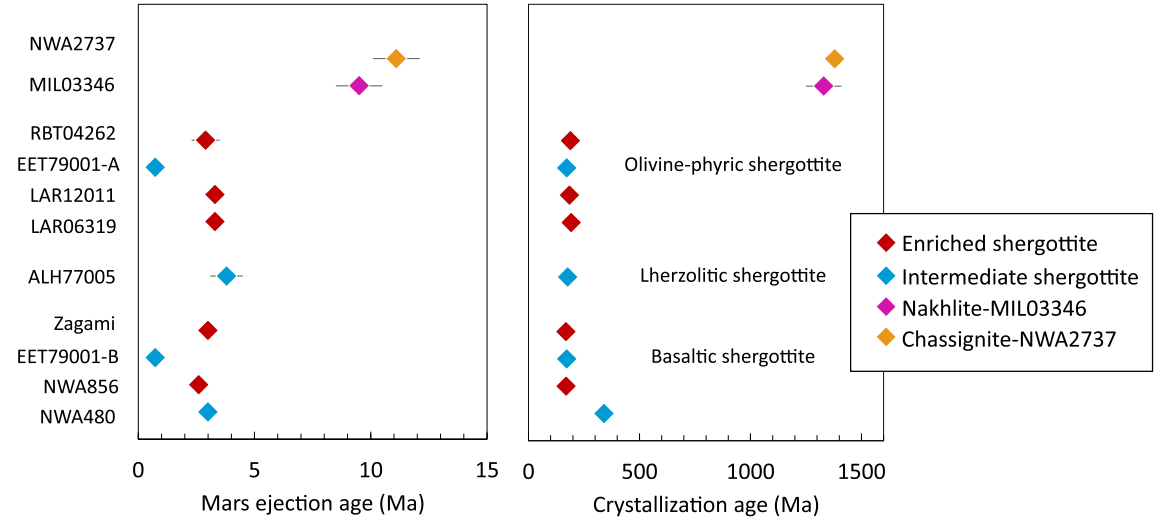

Fig. 1. Crystallization age and Mars ejection age of the 12 samples analyzed in this study, "enr" is for enriched and "interm" is for intermediate shergottite. Data are taken from the review of McSween and McLennan, (2014) and Bellucci et al. (2015) for the crystallization age of LAR12011 (see Supplementary Materials).

surface was sufficiently long (Hin et al., 2017; Young et al., 2019; Tang and Young 2020). Since we are investigating Si isotope differences among mantle reservoirs, the main issue is to find out whether the various reservoirs formed at different depths could have experienced various degrees of Si loss leading to Si isotope fractionation. In this case, one would expect a correlation between volatile element loss and $\delta^{30}Si$ in these reservoirs. One possible indicator of such a loss would be the ratio of a moderately volatile element to a more refractory element of similar behavior in magmatic processes, such as melting or crystallization. However, Zn/Fe, Rb/Ba and, Cs/Ba ratios for SNC show no correlation with $\delta^{30}Si$ (Fig. S3), suggesting that this interpretation cannot explain the variations in Si isotopes among SNC meteorites. Thus, although one cannot preclude a global shift in $\delta^{30}Si$ relative to an initially unknown Si isotope composition for the bulk Mars, the existence of mantle heterogeneity seems unrelated to volatile loss.

4.4. Silicon behaviour during magma ocean crystallisation

The ^{182}W and ^{142}Nd isotope signature of martian rocks clearly indicates that mantle convection did not entirely rehomogenize the mantle following magma ocean crystallization (e.g. Foley et al., 2005; Debaille et al., 2007; Caro et al., 2008; Kruijer et al., 2017). Given that Si isotopes have been shown to fractionate between various high-pressure minerals and melts (Méheut and Schauble, 2014; Huang et al., 2014; Qin et al., 2016), it is possible that crystallization of high-pressure minerals in equilibrium with silicate melts could have generated unusual Si isotope signatures.

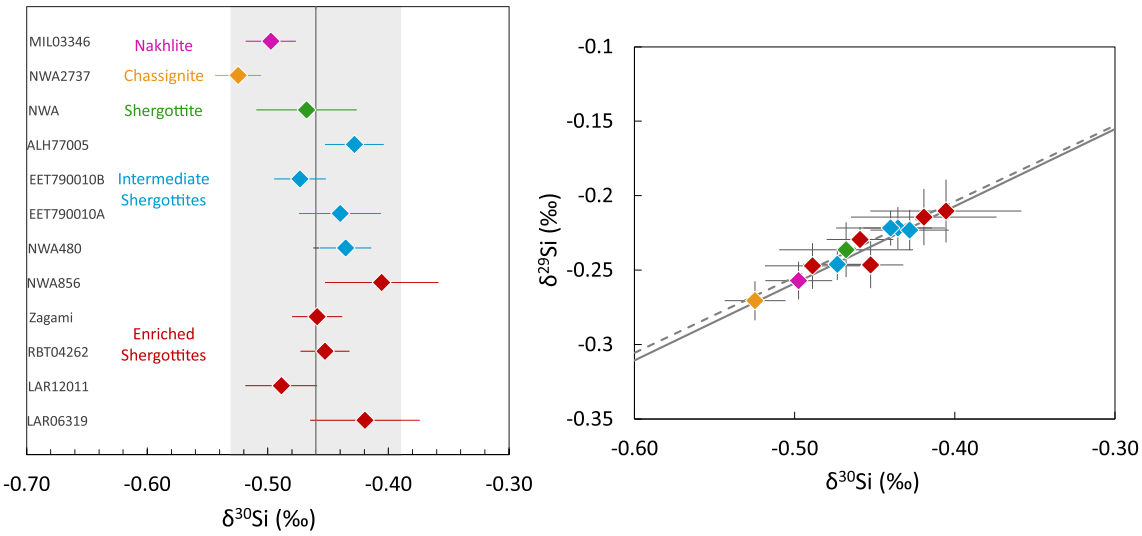

Fig. 2. (a) Si isotope composition of the 12 martian meteorites measured in this study reported as δ^{30}Si. The error bars correspond to the 2SE uncertainty. The shaded area corresponds to the 2SD of all samples and shows the limited dispersion of our data. (b) Three-isotope plot illustrating the mass dependence of our Si isotope measurements (same color symbols as in (a)). The grey solid line represents equilibrium isotope fractionation (slope 0.5178) and the dashed line kinetic isotope fractionation (slope 0.5092).

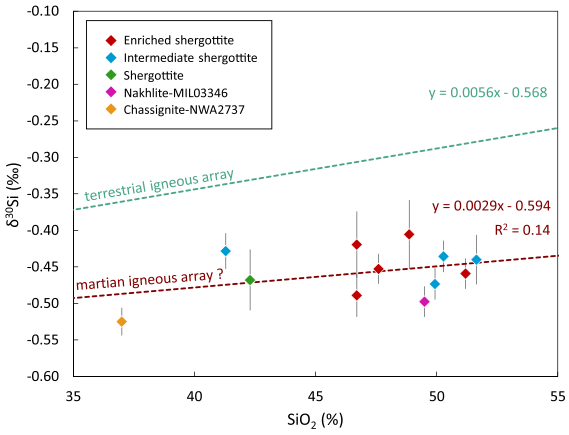

Fig. 3. Variation of the Si isotope composition of SNC meteorites as a function of silica content. The dotted green line corresponds to the "terrestrial igneous array" defined in Savage et al. (2011).

The mass-dependent inter-mineral silicon isotope fractionation between minerals has been shown to depend on melt polymerization, Si-O bond lengths and Si coordination number in minerals and melts (Méheut and Schauble, 2014; Huang et al., 2014; Qin et al., 2016). Using ab initio methods to calculate Si isotope fractionation factors between mineral phases crystallizing from a terrestrial magma ocean, Huang et al. (2014) showed that the terrestrial lower mantle should be lighter than the upper mantle with $\Delta^{30}Si_{upper\ mantle\ -\ lower\ mantle}$ ranging between 0.08 ‰ to 0.12 ‰. However, in the case of the Earth's mantle, the more vigorous convection may have erased these early signatures, which is perhaps not the case in Mars (Kieffer, 2003; Maurice et al., 2017). Following an approach similar to Huang et al. (2014), we investigate in what follows the possible effect of magma ocean crystallization on the Si isotope composition of SNC meteorites.

4.4.1. Crystallization sequence

Models of magma ocean crystallization were developed based on the crystallization sequence described in the study of Draper et al. (2005). This model involves the crystallization of a ~2000 km deep magma ocean and implies mineral phases such as olivine and its high-pressure equivalent (γ-olivine or ringwoodite), pyroxenes (px), garnet and ilmenite (Table 6). A thin layer of perovskite with garnet and magnesiowüstite might be present at the very bottom of the martian mantle (Bertka and Fei, 1997) and its impact on silicon isotope signature will also be discussed. The goal of investigating the possible role of Mg-perovskite was justified by (1) the fact that Mg-perovskite should impart a very clear Si isotope signature and (2) the intention of verifying that Mg-perovskite was indeed unlikely to be a representative phase in the crystallization of the MMO as suggested by recent studies based on completely different approaches.

At each crystallization stage, the mineral assemblage is assumed to be in chemical equilibrium with the surrounding melt before being isolated from the residual melt and the melt is assumed to be chemically homogeneous due to vigorous convection of the molten mantle (Solomatov, 2000; Elkins-Tanton et al., 2003). Various geochemical models have been proposed for the crystallization of magma oceans for the Earth or Mars and the model presented here is inspired from previous work (e.g. Caro et al., 2005; Debaille et al., 2008; Rizo et al., 2011) but adapted

Table 6
Models of martian magma ocean crystallisation.

Crystallisation sequence from	Stage#	Percent solid (%)	Mineral phases
Draper et al. (2005)	5	98	cpx + ilmenite (90:10)
	4	90	opx + cpx (60:40)
	3	65	olivine + opx (50:50)
	2	35	ringwoodite + majorite (95:5)
	1	10	majoritic garnet
Crystallisation sequence from	**Stage#**	**Percent solid (%)**	**Mineral phases**
Draper et al. (2005) + pv	6	98	cpx + ilmenite (90:10)
	5	90	opx + cpx (60:40)
	4	65	olivine + opx (50:50)
	3	35	ringwoodite + majorite (95:5)
	2	10	majoritic garnet
	1	5	pv + majorite + mw (64:20:16)

"pv" stands for perovskite and "mw" for magnesiowüstite.

for the case of stable isotopes. The Si isotope composition of the residual melt R_{melt} was calculated using a mass-balance equation at each crystallization stage according to:

$$R_0 = F_{melt} \times R_{melt} + \sum_i F_i \times R_i \quad (2)$$

R_0 and R_i are respectively the $^{30}Si/^{28}Si$ isotope ratio of the bulk magma ocean (minerals + melt) and of mineral phase i; F_i corresponds to the mass fraction of silicon in mineral i, while F_{melt} is the mass fraction of Si in the melt. This mass balance equation can be rewritten with the delta notation to calculate the δ^{30}Si of the melt and each mineral phase as follows:

$$\delta^{30}Si_{melt} = \delta^{30}Si_0 - \sum_i F_i \times {}^{30}Si_{mineral\ \ i-melt} \quad (3)$$

where

$$\Delta^{30}Si_{mineral\ \ i-melt} = \delta^{30}Si_{mineral\ \ i} - \delta^{30}Si_{melt} \quad (4)$$

The initial composition of the magma ocean $\delta^{30}Si_0$ was supposed to be equal to the mean isotope composition of the SNC, i.e. −0.46 ± 0.07 ‰. For the second step of crystallization, $\delta^{30}Si_0$ corresponded to the isotope composition of the residual melt. The δ^{30}Si of each mineral was calculated from the definition of $\Delta^{30}Si_{mineral\ i-melt}$. The Si isotope composition of cumulates were calculated with the following equation:

$$\delta^{30}Si_{cumulate} = \sum_i F_i \times \delta^{30}Si_{mineral\ \ i} / \sum_i F_i \quad (5)$$

The mass fraction of Si in each mineral phase F_i ($m^{Si}_{\min i}$ / m^{Si}_{bulk}) was calculated according to the following equation:

$$F_i = \frac{D_{\min i} \times X_i}{\sum_j D_{\min j} \times X_j + X_{melt}} \quad (6)$$

The mass fraction of each phase X_i is calculated at each crystallization stage (Table 6). Note that Table 6 includes a version of the model including perovskite in order to test whether perovskite could be a liquidus phase to check the consistency of Si isotope observations with previous inferences (e.g. Yoshizaki and McDonough 2020). The partition coefficients of silicon between mineral and melt $D_{\min j}$ were obtained from the literature and are summarized in Table S3 (Borg and Draper, 2003; Corgne et al., 2005).

4.4.2. Si isotope fractionation factor between mineral and melt

Huang et al. (2014) calculated silicon isotope fractionation factors for the following mantle minerals that should be present in the martian mantle: olivine, orthopyroxene, clinopyroxene, majorite, ringwoodite and Mg-perovskite using density functional theory. Huang et al. (2014) have also defined a method for calculating the isotope fraction factor between mineral and melts based on the coordination of Si in melts (See Supplement for details). In this study, we used the coordination of Si in melts determined at various pressures and temperatures for a pyrolite (Solomatova and Caracas, 2019). We then assume as in Huang et al. (2014) that the isotope fractionation factor between a mineral i and IV coordinated Si in the melt is equal to:

$$\Delta^{30}Si_{\min\ \ i-IVSi\ \ melt} = \Delta^{30}Si_{\min\ \ i-olivine} = 1000 \times (ln\beta_{\min\ \ i} - ln\beta_{olivine}) \quad (7)$$

With this type of assumption, one can calculate the isotope fractionation factor between mineral i and melt as a function of temperature. The Si isotope fractionation coefficients were thus calculated at 0 GPa, 10 GPa and 20 GPa. The temperatures were constrained using the crystallization sequences described in Table 6 and the temperature profile of the magma ocean (Elkins-Tanton et al., 2003; Plesa et al., 2014).

4.4.3. Silicon isotope composition of martian mantle reservoirs

The results of the magma ocean crystallisation models for Si isotopes are shown in Figs. 4 and 5 and reported in Table 7 that represents the calculated δ^{30}Si of the bulk cumulates, as well as the δ^{30}Si of the residual melt calculated at each crystallisation stage (see Table S6 and Table S7 for calculated δ^{30}Si in individual mineral phases and the corresponding Si isotope fractionation factors).

According to our model, the crystallization of the magma ocean should lead to the formation of heterogeneous mantle cumulate reservoirs with respect to their Si isotope compositions as shown in Table 7. The "high pressure" mineral phases, i.e. majorite and ringwoodite, were enriched in light silicon isotopes compared with the melt, in agreement with isotope fractionation studies of high-pressure mineral phases (Huang et al., 2014). The δ^{30}Si of bulk cumulates ranges between −0.354 ‰ and −0.506 ‰, which agrees with the range found in SNC meteorites. If one assumes that there is an Mg-perovskite layer of approximately 360 km at the very bottom of the magma ocean representing 5 wt% of solid (Bertka and Fei, 1997), then the calculated cumulates have a very light δ^{30}Si value of −0.79 ‰ (Table 7). Since there is no evidence of such extreme δ^{30}Si in SNC meteorites, this suggests that this reservoir was never sampled by martian magmatism. The sampling of a deep reservoir would require specific conditions (as described for Fe isotopes in Williams et al., 2021). First, the deep-seated cumulates with a low δ^{30}Si value must be entrained to a high enough level for melting and second, the melting process must preserve the specific Si isotope signature (which is likely in this case as there is little fractionation between mineral and melts in the upper mantle). Since there are indications of mantle plume magmatism (Kieffer, 2003; Day et al., 2018) and efficient convection in the martian mantle (Kieffer, 2003), (despite evidence for the preservation of isotope heterogeneities), we consider it more likely that this reservoir does not exist in the martian mantle.

If later processes such as mantle melting and fractional crystallization had little influence on the δ^{30}Si values, then the δ^{30}Si of bulk cumulates can be directly compared with those of SNC meteorites. The δ^{30}Si of our SNC samples is overall within the range of the calculated δ^{30}Si range of cumulates (except for the Mg-perovskite-bearing cumulate). If the pressure of the core-mantle boundary were deeper than 22.5 GPa (Bertka and Fei 1997), the bottom of the magma ocean should have included a layer of Mg-perovskite (bridgmanite) with a markedly low δ^{30}Si value. Since no SNC meteorites carry such a signature, we conclude that there is no evidence for a bridgmanite layer at the bottom of the martian mantle. This observation is consistent with the recent finding that

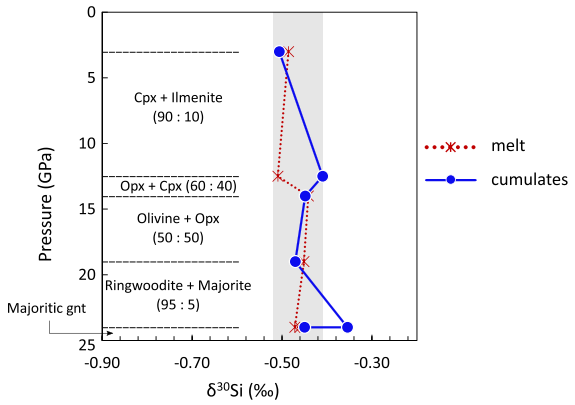

Fig. 4. δ^{30}Si values of cumulates and residual melts in the martian mantle as a function of the pressure of magma ocean crystallization in GPa using the various mineralogical assemblages given in Table 6. This model is based on the crystallisation sequence of Draper et al. (2005). The plotted curves correspond to the δ^{30}Si of the cumulate and the melt that are in equilibrium at each pressure.

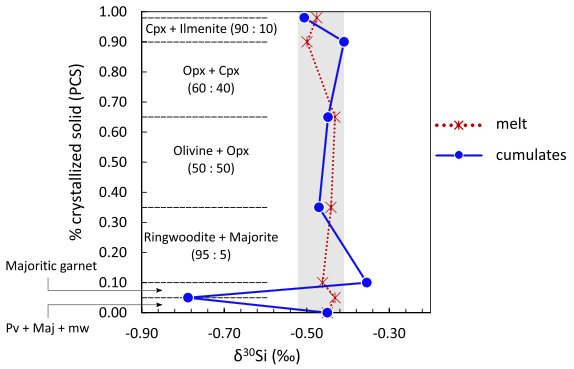

Fig. 5. Silicon isotope composition of cumulates and residual melts in the martian mantle after magma ocean crystallization based on the crystallization sequence of Draper et al. (2005) as a function of the crystallized fraction, assuming that Mg-perovskite is stable in the first cumulate. The shaded blue rectangle shows the range in δ^{30}Si of SNC meteorites. The plotted curves correspond to the δ^{30}Si of the cumulate and the melt that are in equilibrium for a given percent of crystallized solid (PCS).

the core of Mars had a radius of 1830 ± 40 km, precluding the existence of a Mg-perovskite layer at the core-mantle boundary (Stähler et al., 2021). Altogether, this model also suggests that the magma ocean crystallization model may be consistent with our observations. One could speculate that if such a perovskite had formed near the core mantle boundary, it would likely have been replaced by an iron-rich basal layer as described in Samuel et al. (2021). Had it existed, this means that the perovskite layer would have been unlikely to remain a hidden reservoir. Our modelling shows that the existence of measurable Si isotope fractionation resulting from magma ocean crystallization hinges on the coexistence of Si(IV), Si(V) and Si(VI) in high pressure minerals and melts (Huang et al., 2014; Solomatova and Caracas, 2019). This is the case of majorite and bridgmanite (Mg-perovskite) but significant fractionation can result also from ringwoodite. These effects are unlikely to be found in smaller planetary objects such as Vesta or the Moon, where the pressure at the core-mantle boundary is ≤ 5GPa.

To further investigate whether the observed Si isotope signatures could correspond to mantle reservoirs formed during magma ocean crystallisation, our model was used to calculate the Sm/Nd signature of the cumulates, as this ratio can be compared with Sm/Nd estimates of source composition, based on ^{147}Sm-^{143}Nd systematics in SNC meteorites.

4.5. Sm-Nd fractionation during magma ocean crystallization

Elemental ratios of incompatible trace elements can be useful tracers of magma ocean crystallization, as the high-pressure phases typical of magma ocean crystallization may impart signatures that differ from those of typical mantle-crust evolution (Kato et al., 1988; Caro et al., 2005; Rizo et al., 2011; Jackson et al., 2014). In order to assess the effect of magma ocean crystallization in Mars, the partitioning of Sm and Nd at each magma ocean crystallization stage was calculated using the same formalism as described in section 4.3. The composition of each mineral phase within the resulting cumulate and of the residual melt was calculated following the crystallisation sequences described in Table 6 using crystal-melt partition coefficients determined in previous studies (Dunn and Sen, 1994; Borg and Draper, 2003; Corgne and Wood, 2004; Corgne et al., 2005, 2012; Mallmann and O'Neill, 2009).

For example, the concentration of Nd in a mineral i, $C^{Nd}_{min\ i}$ was calculated as:

$$C^{Nd}_{min\ i} = D^{Nd}_{min\ i} \times C^{Nd}_0 / (\sum_i X_i \times C^{Nd}_{min\ i} + X_{melt}) \quad (8)$$

with

$$C^{Nd}_{melt} = C^{Nd}_{min\ i} / D^{Nd}_{min\ i} \quad (9)$$

and X_i representing the mass fraction of each phase; $D^{Nd}_{min\ i}$ the partition coefficient of Nd between a mineral i and the melt; C^{Nd}_0 the initial concentration of Nd in the magma ocean (Taylor, 2013) for the first crystallisation stage and of the residual melt for the following crystallisation stages. By analogy with the calculation of Si isotope compositions of cumulates, the distribution of REE in the cumulates was calculated as follows:

$$C^{Nd}_{cumulates} = \sum_i X_i \times C^{Nd}_{min\ i} / \sum_i X_i \quad (10)$$

In this study, we focused on the Sm-Nd system since it is an unequivocal tracer of silicate differentiation, in particular magma ocean crystallization (e.g., Debaille et al., 2008). The ^{142}Nd-^{143}Nd record of SNC meteorites indicates that there has been an early Sm/Nd fractionation that is commonly attributed to magma ocean differentiation (Debaille et al., 2007; Caro et al., 2008; Debaille et al., 2008). Similarly to Si isotopes, Sm/Nd ratios are sensitive to high pressure phases such as majorite or Mg-perovskite. Thus, a correlation of Sm/Nd ratios with Si isotopes could be a good indicator of magma ocean differentiation.

The variations in Sm-Nd in SNC meteorites have been interpreted by the mixing of a depleted mantle component and an enriched component that represent either a crustal material (Humayun et al., 2013) or the residual liquid of magma ocean crystallization (Blichert-Toft et al., 1999; Borg and Draper, 2003; Debaille et al., 2007; 2008). As shown in Armytage et al. (2018), the mixing line between depleted mantle and early martian crust represented by the NWA 7034 meteorite does not fit the other SNC data. In addition, this interpretation is also not favoured by Os isotope data in shergottites (Brandon et al., 2012). Thus, the enriched component as a residual liquid or at least ancient mantle heterogeneity (Ferdous et al., 2017) seems most consistent with existing data.

Owing to its lower ionic radius than Nd, Sm is more compatible than Nd in minerals relative to silicate melts. Thus, upon crystallizing the martian magma ocean, it is expected that the effect of MMO crystallization will be to fractionate the Sm/Nd ratio with a higher

Table 7
Si isotope composition of the martian mantle corresponding to the crystallization stages of Table 6.

	Model		Model + Mg-pv	
	δ^{30}Si cumulate (‰)	δ^{30}Si melt (‰)	δ^{30}Si cumulate (‰)	δ^{30}Si melt (‰)
Stage 6			−0.51	−0.48
Stage 5	−0.51	−0.49	−0.41	−0.50
Stage 4	−0.41	−0.51	−0.45	−0.43
Stage 3	−0.45	−0.44	−0.47	−0.44
Stage 2	−0.47	−0.45	−0.35	−0.46
Stage 1	−0.35	−0.47	−0.79	−0.43

Sm/Nd in the residual melt, while the cumulate phases will be characterized by a higher Sm/Nd ratio. In order to examine the effect of magma ocean crystallization on Sm/Nd fractionation, one cannot consider the Sm/Nd directly measured in the samples, as this ratio could have been modified by the process of partial melting and fractional crystallization that affected all magmas. Thus, rather than using the Sm/Nd measured in SNC meteorites, we calculated the integrated $^{147}Sm/^{144}Nd$ ratio of their mantle source based on their ^{143}Nd isotope signature. An approach combining ^{142}Nd and ^{143}Nd data is also possible. However, by using only ^{143}Nd, it is possible to calculate an Sm/Nd_{source} ratio for all samples. First, the present-day $^{143}Nd/^{144}Nd$ isotope ratio, together with the measured $^{147}Sm/^{144}Nd$ (Borg et al., 2016; Borg and Draper, 2003; Caro et al., 2008; Nyquist and Reese, 2009; Kruijer et al., 2017) and crystallisation age of the sample (see Supplementary Materials) are used to calculate the $^{143}Nd/^{144}Nd$ isotope ratio at the time of eruption (formation):

$$\frac{^{143}Nd}{^{143}Nd_{present}} = \frac{^{143}Nd}{^{144}Nd_{T_{erupt}}} + \left(\frac{^{147}Sm}{^{144}Nd}\right)_{sample}\left(e^{\lambda T_{erupt}} - 1\right) \quad (11)$$

Hence:

$$\frac{^{143}Nd}{^{144}Nd_{T_{erupt}}} = \frac{^{143}Nd}{^{143}Nd_{present}} - \left(\frac{^{147}Sm}{^{144}Nd}\right)_{sample}\left(e^{\lambda T_{erupt}} - 1\right) \quad (12)$$

We now assume that this sample evolved from a chondritic Nd isotope composition starting from the beginning of the Solar System at 4568 Ma (Bouvier and Wadhwa, 2010) until the time of eruption (T_{erupt}):

$$\frac{^{143}Nd}{^{144}Nd_{T_{erupt}}} = \frac{^{143}Nd}{^{144}Nd_{T_0}} + \frac{^{147}Sm}{^{144}Nd_{source}}\left(e^{\lambda T_0} - e^{\lambda T_{erupt}}\right) \quad (13)$$

From these equations, it is possible to derive the $^{147}Sm/^{144}Nd$ ratio of the source of SNC meteorite samples:

$$\frac{^{147}Sm}{^{144}Nd_{source}} = \frac{\frac{^{143}Nd}{^{144}Nd_{T_{erupt}}} - \frac{^{143}Nd}{^{144}Nd_{T_0}}}{e^{\lambda T_0} - e^{\lambda T_{erupt}}} \quad (14)$$

The calculated $^{147}Sm/^{144}Nd$ ratio of the SNC sources are given in Table 8 and these ratios are plotted as a function of $\delta^{30}Si$ in Fig. 6. The $\delta^{30}Si$ values are negatively correlated with $^{147}Sm/^{144}Nd_{source}$ for the SNC meteorites characterized by a high Sm/Nd ratio. In contrast, the enriched shergottites with a low Sm/Nd show no correlation with $\delta^{30}Si$ values.

The SNC data can then be compared with the calculated melt and cumulate compositions during magma ocean crystallization using the model described above. The results are plotted in Fig. 7 and it is obvious that the cumulate composition shows a much broader range in Sm/Nd and $\delta^{30}Si$ than what is observed in SNC meteorites. As shown in the next section, by including the effect of trapping melts in the cumulates, the observations can be made more consistent with the model predictions.

Table 8
Calculated $^{147}Sm/^{144}Nd$ present-day ratios of the sources, sh-shergottite, ol phyr-olivine-phyric, lh-lherzolitic and interm for intermediate.

Sample name	Type	$^{147}Sm/^{144}Nd$ (source)
LAR06319	enriched-ol phyr sh	0.1845
LAR12011	enriched-ol phyr sh	0.1840
RBT04262	enriched-ol phyr sh	0.1849
Zagami	enriched-sh	0.1844
NWA856	enriched-sh	0.1849
ALH77005	interm-lh sh	0.2164
NWA480	interm-sh	0.2166
EET790010A	interm-sh	0.2234
EET790010B	interm-sh	0.2258
MIL03346	nakhlite	0.2330
NWA2737	chassignite	0.2371

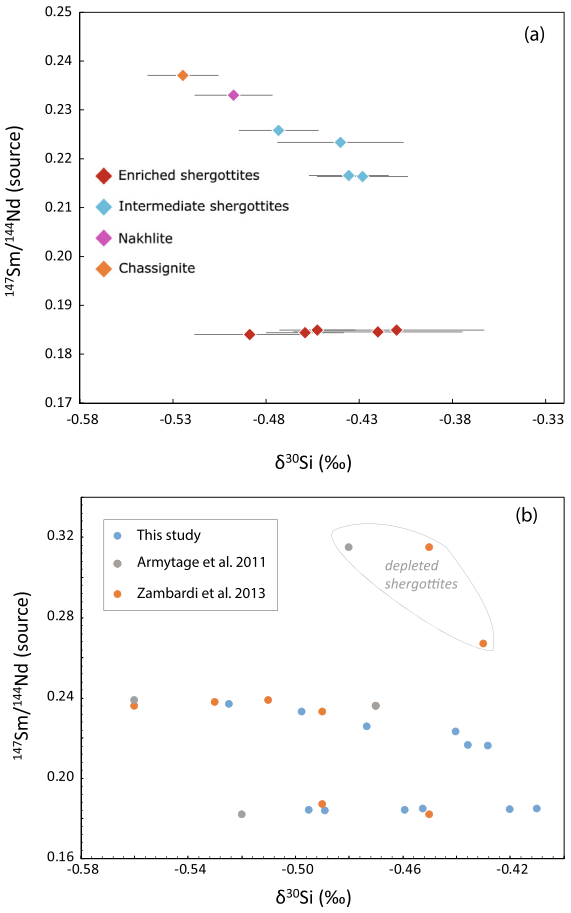

Fig. 6. (a) Variations in silicon isotope compositions of SNC with the calculated $^{147}Sm/^{144}Nd$ of their mantle sources. (b) Variations in silicon isotope compositions of SNC with the calculated $^{147}Sm/^{144}Nd$ of their mantle sources including data from this study and literature data from Armytage et al. (2011) and Zambardi et al. (2013). The intermediate shergottites combined with Nakhlites and Chassigny yield a coherent trend, while the enriched shergottites give a flat trend.

4.6. A role for trapped melt in the martian magma ocean cumulate pile

It has been advocated in previous studies of magma ocean crystallization, that depending on the relative rates of cooling and cumulate pile compaction, that some residual melt could be trapped within the cumulate pile (Elkins-Tanton et al., 2003). According to Elkins-Tanton et al. (2003), melts can be trapped in solidifying cumulate piles if the solidus is reached before melt escapes due to crystal mush compaction. The net result of trapping melts in a cumulate is to buffer the crystal + melt composition to a narrower range, since the trapped melt has the same composition as the residual melt. Such a model was used in the study of Debaille et al. (2008) to demonstrate that the ^{176}Lu-^{176}Hf and Sm-Nd systematics of shergottites requires a mixture between a residual melt (i.e. a trapped melt) and depleted cumulates. Note that the composition of the trapped melt in the model of Debaille et al. (2008) corresponded to residual melt formed after 98–99.5 % equilibrium crystallization.

Here, the melt trapped in cumulates is the melt formed at each individual stage of crystallization. The trapped melt can simply be considered as an additional 'mineral phase' with a mineral/melt partition coefficient of 1. The calculation of the melt composition is identical to the previous case. The only difference is in the composition of the cumulates. In this case, the Si isotope composition of the cumulate can be calculated as:

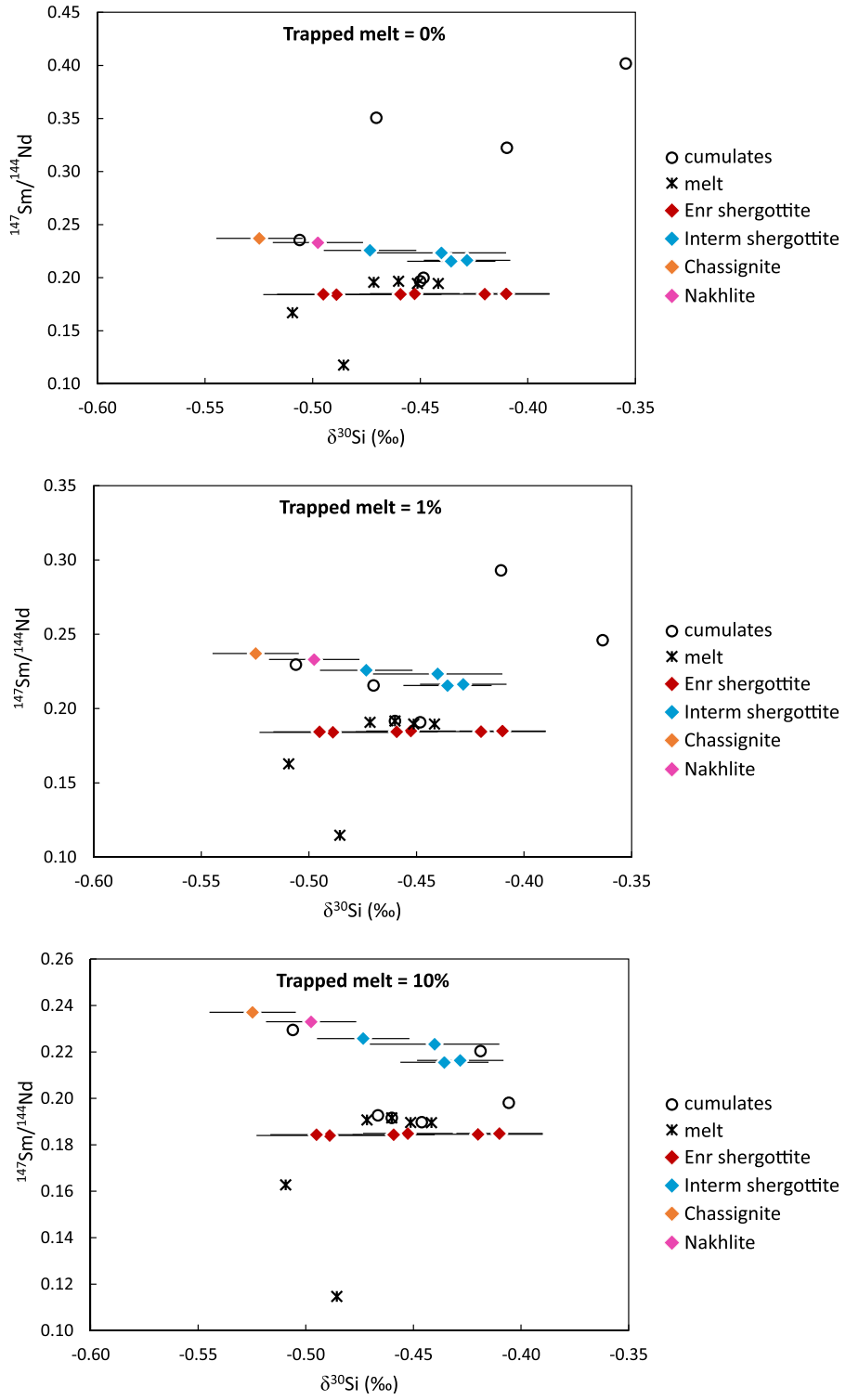

Fig. 7. $^{147}Sm/^{144}Nd$ versus $\delta^{30}Si$ in cumulates and residual melts calculated using a magma ocean crystallization model based on the crystallization sequence of Draper et al. (2005) for various mass fractions of trapped melt in the cumulate pile (a) trapped melt = 0 % (b) trapped melt = 1 % (c) trapped melt = 10 %. The mass fraction of trapped melt is assumed to be equal to 0 % in the top crystallized layer. The data for SNC meteorites from this study is shown for reference.

$$\delta^{30}Si_{cumulate} = \frac{\delta^{30}Si_0 - F'_{melt}\delta^{30}Si_{melt}}{1 - F'_{melt}} \quad (15)$$

where F'_{melt} represents the mass fraction of melt not being trapped in cumulate. The mass fraction of trapped melt is then expressed as:

$$F_{trapped} = F_{melt} - F'_{melt} \quad (16)$$

The mass fraction of trapped melt is not known a priori and is commonly taken as ranging between 1 and 10 % (e.g. Charlier et al., 2018; Kraettli et al., 2022) in the case of magma ocean crystallization. If one introduces the effect of trapping melts inside cumulates (Fig. 7), then there is a reasonable match between the SNC data and model predictions, especially when the fraction of trapped melt reaches 10 %. As shown in Fig. S2, the match is also

good when all the literature data is included; in particular the depleted shergottites are well explained by a trapped melt fraction of ~1 %, which is consistent with previous studies (e.g. Debaille et al., 2008). The most enriched cumulate and the residual melts, corresponding to the last stages of crystallization give $^{147}Sm/^{144}Nd$ and $\delta^{30}Si$ values that are overall consistent with enriched shergottites, while the intermediate and depleted shergottites are explained by cumulates formed at greater depths.

The $^{147}Sm/^{144}Nd$ ratio of the sources of intermediate shergottites, nakhlite sample MIL03346 and chassignite sample NWA2737 characterized by $^{147}Sm/^{144}Nd_{source}$ greater than the chondritic value show a negative correlation with their $\delta^{30}Si$, which agrees with the predicted negative trend observed between the different mantle sources (see Fig. 6). The measured $\delta^{30}Si$ variations in these mantle-derived samples can be attributed to magma ocean crystallization rather than magmatic differentiation, which is consistent with the lack of a correlation between the $\delta^{30}Si$ and the SiO_2 concentrations and other direct indicators of magmatic processes.

Unfortunately, there is not enough ^{182}W data available in the literature on the same samples measured in this study to further document our inference as we have only three samples measured in common with the studies of Foley et al. (2005) and Kruijer et al. (2017).

4.7. The origin of enriched shergottites

The predicted composition of the enriched melt produced by magma ocean crystallization agrees with the observed $\delta^{30}Si$ and Sm/Nd_{source} of enriched SNC meteorites, as shown in Fig. 7. However, one intriguing observation is the rather constant Sm/Nd with variable $\delta^{30}Si$. The predicted Sm/Nd in residual melts are also more variable than the range in enriched shergottites; thus, it suggests that either one type of melt was sampled in SNC meteorites or that in terms of Sm/Nd, there has been homogeneization in the enriched shergottite reservoir. In both cases, one would expect constant $\delta^{30}Si$ values. One interpretation might be that the $\delta^{30}Si$ variations in enriched shergottites are of secondary nature and thus unrelated to magma ocean crystallization.

For example, one could speculate that fluid-rock interactions could have modified Si isotopes during recent events without affecting the long term Sm/Nd systematics. If we assume that aqueous alteration could have taken place at the surface or or subsurface of Mars, then it is possible that alteration or weathering would have enriched crustal rocks in light Si isotopes (as observed in Iceland basalts by Georg et al., 2006).

Enriched shergottites are also known to be more oxidized than depleted shergottites and this property may indirectly affect Si isotope evolution. It has been shown that silicate polymerization is modified by the redox state of magmas (e.g. Mysen et al., 1984) with oxidized magma being more depolymerized. It has been documented that enriched shergottites are characterized by greater fO_2 (Herd, 2003), although this interpretation has recently been questioned (Nicklas et al., 2021). Thus, one could imagine that the corresponding modification of melt structure directly affecting the bond length of Si-O in the melt could directly impact the $\delta^{30}Si$ of magmas. The observed $\delta^{30}Si$ variations are small, which means that such an effect was perhaps not detected in previous studies.

In summary, the enriched shergottites may have been affected by a different set of processes that could be related to the more oxidized nature of these samples or to fluid-rock interactions if the source of these samples was indeed residing in the martian crust or lithosphere.

5. Conclusions

The Si isotope composition of SNC meteorites shows a small but resolvable variation with $\delta^{30}Si$ values ranging between −0.41 and −0.52 ‰. No correlation was observed between major elements and silicon isotopes and this may be due to the complex magmatic history of SNC rocks, including the effects of magma ocean crystallization, partial melting and fractional crystallization. Similarly, the $\delta^{30}Si$ values show no correlation with indicators of volatile element loss that should have been observed if there had been different degrees of volatile loss during an early magma ocean vaporization.

The effect of the crystallization of a magma ocean on Si isotopes was investigated and compared with the observed $\delta^{30}Si$ variations in SNC. First, the crystallization in the presence of Mg-perovskite (bridgmanite) at the bottom of the martian mantle should have produced much lower $\delta^{30}Si$ values than what is observed. Our observations are thus consistent with the recent finding of a large core for Mars, precluding the stability of Mg-perovskite near the core-mantle boundary. However, we did find a correlation with $^{147}Sm/^{144}Nd$ estimates of the SNC mantle sources with $\delta^{30}Si$ for the most depleted samples, while the enriched rocks showed no trend. The variations in $\delta^{30}Si$ are attributed to changes in Si coordination in high pressure minerals formed during magma ocean crystallization, relative to the mean coordination of the silicate melt in equilibrium with these minerals. The correlation of $\delta^{30}Si$ with $^{147}Sm/^{144}Nd_{source}$ can be explained by ancient mantle heterogeneities resulting from magma ocean crystallization and the formation of cumulates that includes some of the local residual melt.

The enriched shergottite samples displayed a significant range in $\delta^{30}Si$ values despite having a constant Sm/Nd ratio. This singular behaviour was attributed either to Si isotope fractionation related to change in coordination in the derived enriched melts or to fluid-rock interactions.

More data on the most depleted shergottites and on a common data set including Hf/W data would be useful to fully assess our inferences regarding the role of a magma ocean on the Si isotope signature of martian rocks.

Data availability

We have shared the data upon submission

Declaration of Competing Interest

The authors declare that they have no known competing financial interests or personal relationships that could have appeared to influence the work reported in this paper.

Acknowledgements

This study was funded by the ERC Advanced Grant COSMOKEMS #694819. We thank Chloé Michaut and Harry Becker for discussions. We thank the Museum National d'Histoire Naturelle (Paris) for providing the Zagami meteorite and NASA for providing SNC meteorites and CAPTEM for providing lunar sample 70017. We thank two anonymous reviewers and the Associate Editor Helen Williams for their constructive comments that greatly helped improve this manuscript.

Appendix A. Supplementary material

Supplementary material to this article can be found online at https://doi.org/10.1016/j.gca.2022.10.002.

References

Armytage, R.M.G., Georg, R.B., Savage, P.S., Williams, H.M., Halliday, A.N., 2011. Silicon isotopes in meteorites and planetary core formation. Geochim. Cosmochim. Acta 75, 3662–3676.

Armytage, R.M.G., Georg, R.B., Williams, H.M., Halliday, A.N., 2012. Silicon isotopes in lunar rocks: Implications for the Moon's formation and the early history of the Earth. Geochim. Cosmochim. Acta 77, 504–514.
Abraham, K., Opfergelt, S., Fripiat, F., Cavagna, A.-J., De Jong, J.T., Foley, S.F., André, L., Cardinal, D., 2008. δ^{30}Si and δ^{29}Si Determinations on USGS BHVO-1 and BHVO-2 Reference Materials with a New Configuration on a Nu Plasma Multi-Collector ICP-MS. Geostand. Geoanalytical Res. 32, 193–202.
Armytage, R.M.G., Debaille, V., Brandon, A.D., Agee, C.B., 2018. A complex history of silicate differentiation of Mars from Nd and Hf isotopes in crustal breccia NWA 7034, Earth Planet. Sci. Lett. 502, 274–283.
Bellucci, J.J., Nemchin, A.A., Whitehouse, M.J., Snape, J.F., Bland, P., Benedix, G.K., 2015. The Pb isotopic evolution of the Martian mantle constrained by initial Pb in Martian meteorites. J. Geophys. Res. 120, 2224–2240.
Bertka, C.M., Fei, Y., 1997. Mineralogy of the Martian interior up to core-mantle boundary pressures. J. Geophys. Res. Solid Earth 102, 5251–5264.
Blichert-Toft, J., Gleason, J.D., Télouk, P., Albarède, F., 1999. The Lu–Hf isotope geochemistry of shergottites and the evolution of the Martian mantle–crust system. Earth Planet. Sci. Lett. 173, 25–39.
Bogard, D.D., Johnson, P., 1983. Martian Gases in an Antarctic Meteorite? Science 221, 651–654.
Borg, L.E., Brennecka, G.A., Symes, S.J.K., 2016. Accretion timescale and impact history of Mars deduced from the isotopic systematics of martian meteorites. Geochim. Cosmochim. Acta 175, 150–167.
Borg, L.E., Draper, D.S., 2003. A petrogenetic model for the origin and compositional variation of the martian basaltic meteorites. Meteorit. Planet. Sci. 38, 1713–1731.
Bourdon, B., Roskosz, M., Hin, R.C., 2018. Isotope tracers of core formation. Earth Sci. Rev. 181, 61–81.
Bouvier, L.C., Costa, M.M., Connelly, J.N., Jensen, N.K., Wielandt, D., Storey, M., Nemchin, A.A., Whitehouse, M.J., Snape, J.F., Bellucci, J.J., Moynier, F., Agranier, A., Gueguen, B., Schönbächler, M., Bizzarro, M., 2018. Evidence for extremely rapid magma ocean crystallization and crust formation on Mars. Nature 558, 586–589.
Bouvier, A., Wadhwa, M., 2010. The age of the Solar System redefined by the oldest Pb–Pb age of a meteoritic inclusion. Nat. Geosci. 3, 637–641.
Brandon, A.D., Puchtel, I.S., Walker, R.J., Day, J.M.D., Irving, A.J., Taylor, L.A., 2012. Evolution of the martian mantle inferred from the 187Re–187Os isotope and highly siderophile element abundance systematics of shergottite meteorites. Geochim. Cosmochim. Acta 76, 206–235.
Breuer, D., Spohn, T., 2003. Early plate tectonics versus single-plate tectonics on Mars: Evidence from magnetic field history and crust evolution. J. Geophys. Res. 108, 5072.
Caro, G., Bourdon, B., Wood, B.J., Corgne, A., 2005. Trace-element fractionation in Hadean mantle generated by melt segregation from a magma ocean. Nature 436, 246–249.
Caro, G., Bourdon, B., Halliday, A.N., Quitté, G., 2008. Super-chondritic Sm/Nd ratios in Mars, the Earth and the Moon. Nature 452, 336–339.
Chakrabarti, R., Jacobsen, S.B., 2010. Silicon isotopes in the inner Solar System: Implications for core formation, solar nebular processes and partial meltin. . Geochim. Cosmochim. Acta 74, 6921–6933.
Charlier, B., Grove, T.L., Namur, O., Holtz, F., 2018. Crystallization of the lunar magma ocean and the primordial mantle-crust differentiation of the Moon. Geochim. Cosmochim. Acta 234, 50–69.
Clayton, R.N., Mayeda, T.K., 1983. Oxygen isotopes in eucrites, shergottites, nakhlites, and chassignites. Earth Planet. Sci. Lett. 62, 1–6.
Corgne, A., Liebske, C., Wood, B.J., Rubie, D.C., Frost, D.J., 2005. Silicate perovskite-melt partitioning of trace elements and geochemical signature of a deep perovskitic reservoir. Geochim. Cosmochim. Acta 69, 485–496.
Corgne, A., Armstrong, L.S., Keshav, S., Fei, Y., McDonough, W.F., Minarik, W.G., Moreno, K., 2012. Trace element partitioning between majoritic garnet and silicate melt at 10–17GPa: Implications for deep mantle processes. Lithos 148, 128–141.
Corgne, A., Wood, B.J., 2004. Trace element partitioning between majoritic garnet and silicate melt at 25GPa. Phys. Earth Planet. Inter. 143–144, 407–419.
Dauphas, N., Poitrasson, F., Burkhardt, C., Kobayashi, H., Kurosawa, K., 2015. Planetary and meteoritic Mg/Si and δ^{30}Si variations inherited from solar nebula chemistry. Earth Planet. Sci. Lett. 427, 236–248.
Day, J.M.D., Tait, K.T., Udry, A., Moynier, F., Liu, Y., Neal, C.R., 2018. Martian magmatism from plume metasomatized mantle. Nat. Commun. 9, 4799.
Debaille, V., Brandon, A.D., Yin, Q.Z., Jacobsen, B., 2007. Coupled ^{142}Nd–^{143}Nd evidence for a protracted magma ocean in Mars. Nature 450, 525–528.
Debaille, V., Yin, Q.Z., Brandon, A.D., Jacobsen, B., 2008. Martian mantle mineralogy investigated by the ^{176}Lu–^{176}Hf and 147Sm–143Nd systematics of shergottites. Earth Planet. Sci. Lett. 269, 186–199.
Douthitt, C.B., 1982. The geochemistry of the stable isotopes of silicon. Geochim. Cosmochim. Acta 46, 1449–1458.
Ziegler, K., Young, E.D., Schauble, E.A., Wasson, J.T., 2010. Metal–silicate silicon isotope fractionation in enstatite meteorites and constraints on Earth's core formation. Earth Planet. Sci. Lett. 295, 487–496.
Draper, D.S., Borg, L.E. and Agee, C.B., 2005. Crystallization of a martian magma ocean and the formation of shergottite source regions: a less Fe-rich Mars? Lunar Planet. Sci. Conf. XXXVI, abstract #1429.
Draper, D.S., Xirouchakis, D., Agee, C.B., 2003. Trace element partitioning between garnet and chondritic melt from 5 to 9 GPa: implications for the onset of the majorite transition in the martian mantle. Phys. Earth Planet. Inter. 139, 149–169.
Dunn, T., Sen, C., 1994. Mineral/matrix partition coefficients for orthopyroxene, plagioclase, and olivine in basaltic to andesitic systems: A combined analytical and experimental study. Geochim. Cosmochim. Acta 58, 717–733.
Elkins-Tanton, L.T., 2005. Possible formation of ancient crust on Mars through magma ocean processes. J. Geophys. Res. 110, E12S01.
Elkins-Tanton, L.T., 2012. Magma Oceans in the Inner Solar System. Annu. Rev. Earth Planet. Sci. 40, 113–139.
Elkins-Tanton, L.T., Parmentier, E.M., Hess, P.C., 2003. Magma ocean fractional crystallization and cumulate overturn in terrestrial planets: Implications for Mars. Meteorit. Planet. Sci. 38, 1753–1771.
Ferdous, J., Brandon, A.D., Peslier, A.H., Pirotte, Z., 2017. Evaluating crustal contributions to enriched shergottites from the petrology, trace elements, and Rb-Sr and Sm-Nd isotope systematics of Northwest Africa 856. Geochim. Cosmochim. Acta 211, 280–306.
Filiberto, J., 2017. Geochemistry of Martian basalts with constraints on magma genesis. Chem. Geol. 466, 1–14.
Fitoussi, C., Bourdon, B., 2012. Silicon isotope evidence against an enstatite chondrite Earth. Science 335, 1477–1480.
Fitoussi, C., Bourdon, B., Kleine, T., Oberli, F., Reynolds, B.C., 2009. Si isotope systematics of meteorites and terrestrial peridotites: implications for Mg/Si fractionation in the solar nebula and for Si in the Earth's core. Earth Planet. Sci. Lett. 287, 77–85.
Foley, C.N., Wadhwa, M., Borg, L.E., Janney, P.E., Hines, R., Grove, T.L., 2005. The early differentiation history of Mars from ^{182}W–^{142}Nd isotope systematics in the SNC meteorites. Geochim. Cosmochim. Acta 69, 4557–4571.
Georg, R.B., Reynolds, B.C., Frank, M., Halliday, A.N., 2006. New sample preparation techniques for the determination of Si isotopic compositions using MC-ICPMS. Chem. Geol. 235, 95–104.
Georg, R.B., Halliday, A.N., Schauble, E.A., Reynolds, B.C., 2007. Silicon in the Earth's core. Nature 447, 1102–1106.
Gessmann, C.K., Wood, B.J., Rubie, D.C., Kilburn, M.R., 2001. Solubility of silicon in liquid metal at high pressure: implications for the composition of the Earth's core. Earth Planet. Sci. Lett. 184, 367–376.
Harper, C.L.H., Nyquist, L.E., Bansal, B., Wiesmann, H., Shih, C.Y., 1995. Rapid Accretion and Early Differentiation of Mars Indicated by ^{142}Nd/^{144}Nd in SNC Meteorites. Science 267, 5.
Herd, C.D.K., 2003. The oxygen fugacity of olivine-phyric martian basalts and the components within the mantle and crust of Mars. Meteorit. Planet. Sci. 38, 1793–1805.
Hin, R.C., Fitoussi, C., Schmidt, M.W., Bourdon, B., 2014. Experimental determination of the Si isotope fractionation factor between liquid metal and liquid silicate. Earth Planet. Sci. Lett. 387, 55–66.
Hin, R.C., Coath, C.D., Carter, P.J., Nimmo, F., Lai, Y.J., Pogge von Strandmann, P.A.E., Willbold, M., Leinhardt, Z.M., Walter, M.J., Elliott, T., 2017. Magnesium isotope evidence that accretional vapour loss shapes planetary compositions. Nature 549, 511–515.
Huang, F., Wu, Z., Huang, S., Wu, F., 2014. First-principles calculations of equilibrium silicon isotope fractionation among mantle minerals. Geochim. Cosmochim. Acta 140, 509–520.
Humayun, M., Nemchin, A., Zanda, B., Hewins, R.H., Grange, M., Kennedy, A., Lorand, J.P., Goepel, C., Fieni, C., Pont, S., Deldicque, D., 2013. Origin and age of the earliest Martian crust from meteorite NWA 7533. Nature 503, 513–516.
Jackson, C.R.M., Ziegler, L.B., Zhang, H., Jackson, M.G., Stegman, D.R., 2014. A geochemical evaluation of potential magma ocean dynamics using a parameterized model for perovskite crystallization. Earth Planet. Sci. Lett. 392, 154–165.
Javoy, M., Balan, E., Méheut, M., Blanchard, M., Lazzeri, M., 2012. First-principles investigation of equilibrium isotopic fractionation of O- and Si-isotopes between refractory solids and gases in the solar nebula. Earth Planet. Sci. Lett. 319–320, 118–127.
Jones, J.H., 1989. Isotopic relationships among the shergottites, the nakhlites and Chassigny. Lunar Planet. Sci. Conf. Proc. 19, 465–474.
Jones, J.H., 2003. Constraints on the structure of the martian interior determined from the chemical and isotopic systematics of SNC meteorites. Meteorit. Planet. Sci. 38, 1807–1814.
Kato, T., Ringwood, A.E., Irifune, T., 1988. Experimental determination of element partitioning between silicate perovskites, garnets and liquids: constraints on early differentiation of the mantle. Earth Planet. Sci. Lett. 89, 123–145.
Kiefer, W.S., 2003. 2003. Melting in the martian mantle: Shergottite formation and implications for present-day mantle convection on Mars. Meteorit. Planet. Sci. 39, 1815–1832.
Kilburn, M.R., Wood, B.J., 1997. Metal–silicate partitioning and the incompatibility of S and Si during core formation. Earth Planet. Sci. Lett. 152, 139–148.
Kraettli, G., Schmidt, M., Liebske, C., 2022. Fractional crystallization of a basal lunar magma ocean: A dense melt-bearing garnetite layer above the core? Icarus 371, 114699.
Kruijer, T.S., Kleine, T., Borg, L.E., Brennecka, G.A., Irving, A.J., Bischoff, A., Agee, C.B., 2017. The early differentiation of Mars inferred from Hf–W chronometry. Earth Planet. Sci. Lett. 474, 345–354.
Kruijer, T.S., Borg, L.E., Wimpenny, J., Sio, C.K., 2020. Onset of magma ocean solidification on Mars inferred from Mn-Cr chronometry. Earth Planet. Sci. Lett. 542, 116315.
Magna, T., Hu, Y., Teng, F.-Z., Mezger, K., 2017. Magnesium isotope systematics in Martian meteorites. Earth Planet. Sci. Lett. 474, 419–426.

Mallmann, G., O'Neill, H.St.C., 2009. The Crystal/Melt Partitioning of V during Mantle Melting as a Function of Oxygen Fugacity Compared with some other Elements Al, P, Ca, Sc, Ti, Cr, Fe, Ga, Y, Zr and Nb. J. Petrol. 50, 1765–1794.
Maurice, M., Tosi, N., Samuel, H., Plesa, A.-C., Hüttig, C., Breuer, D., 2017. Onset of solid-state mantle convection and mixing during magma ocean solidification. J. Geophys. Res. Planets 122, 577–598.
McCubbin, F.M., Elardo, S.M., Shearer, C.K., Smirnov, A., Hauri, E.H., Draper, D.S., 2013. A petrogenetic model for the comagmatic origin of chassignites and nakhlites: Inferences from chlorine-rich minerals, petrology, and geochemistry. Meteorit. Planet. Sci. 48, 819–853.
McSween, H.Y., 1994. What we have learned about Mars from SNC meteorites. Meteoritics 29, 757–779.
McSween, H.Y., McLennan, S.M., 2014. 2.10 - Mars. In: Holland, H.D., Turekian, K.K. (Eds.), Treatise on Geochemistry. Second ed. Elsevier, Oxford, pp. 251–300.
Méheut, M., Schauble, E.A., 2014. Silicon isotope fractionation in silicate minerals: Insights from first-principles models of phyllosilicates, albite and pyrope. Geochim. Cosmochim. Acta 134, 137–154.
Mysen, O.B., Virgo, D., Seifert, F.A., 1984. Redox equilibria of iron in alkaline earth silicate melts: relationships between melt structure, oxygen fugacity, temperature and properties of iron-bearing silicate liquids. Am. Min. 69, 834–847.
Nicklas, R.W., Day, J.M.D., Vaci, Z., Udry, A., Liu, Y., Tait, K.T., 2021. Uniform oxygen fugacity of shergottite mantle sources and an oxidized martian lithosphere. Earth Planet. Sci. Lett. 564, 116876.
Nimmo, F., Kleine, T., 2007. How rapidly did Mars accrete? Uncertainties in the Hf–W timing of core formation. Icarus 191, 497–504.
Nyquist, L.E., Reese, Y., 2009. Rb-Sr and Sm-Nd studies of olivine-phyric shergottites RBT 04262 AND LAR 06319: isotopic evidence for relationship to enriched basaltic shergottites. In: 40th Lunar and Planet. Sci. Conf., vol. 2.
Papike, J.J., Karner, J.M., Shearer, C.K., Burger, P.V., 2009. Silicate mineralogy of martian meteorites. Geochim. Cosmochim. Acta 73, 7443–7485.
Plesa, A.-C., Tosi, N., Breuer, D., 2014. Can a fractionally crystallized magma ocean explain the thermo-chemical evolution of Mars? Earth Planet. Sci. Lett. 403, 225–235.
Pringle, E.A., Moynier, F., Savage, P.S., Badro, J., Barrat, J.A., 2014. Silicon isotopes in angrites and volatile loss in planetesimals. P. Natl. Acad. Sci. USA 111, 17029–17032.
Pringle, E.A., Savage, P.S., Badro, J., Barrat, J.-A., Moynier, F., 2013. Redox state during core formation on asteroid 4-Vesta. Earth Planet. Sci. Lett. 373, 75–82.
Qin, T., Wu, F., Wu, Z., Huang, F., 2016. First-principles calculations of equilibrium fractionation of O and Si isotopes in quartz, albite, anorthite, and zircon. Contrib. Mineral. Petrol. 171, 91.
Rai, N., van Westrenen, W., 2013. Metal-Silicate Partitioning of Siderophile Elements: Application to Core-mantle differentiation in Mars. J. Geophys. Res. Planets 118, 1195–1203.
Reese, C., Solomatov, V., 2006. Fluid dynamics of local martian magma oceans. Icarus 184, 102–120.
Reynolds, B.C., Aggarwal, J., André, L., Baxter, B., Beucher, C., Brzezinski, M.A., Engström, E., Georg, R.B., Land, M., Leng, M.J., Opfergelt, S., Rodushkin, I., Sloane, H.J., Van den Boorn, S.H.J.M., Vroon, P.Z., Cardinal, D., 2007. An inter-laboratory comparison of Si isotope reference materials. J. Anal. At. Spectrom. J. Anal. At. Spectrom. 22, 561–568.
Righter, K., Chabot, N.L., 2011. Moderately and slightly siderophile element constraints on the depth and extent of melting in early Mars: Siderophile elements and core formation on Mars. Meteorit. Planet. Sci. 46, 157–176.
Righter, K., Drake, M.J., 1996. Core Formation in Earth's Moon, Mars, and Vesta. Icarus 124, 513–529.
Rizo, H., Boyet, M., Blichert-Toft, J., Rosing, M., 2011. Combined Nd and Hf isotope evidence for deep-seated source of Isua lavas. Earth Planet. Sci. Lett. 312, 267–279.
Samuel, H., Ballmer, M., Padovan, S., Tosi, N., Rivoldini, A., Plesa, A.-C., 2021. The thermo-chemical evolution of Mars with a strongly stratified mantle. J. Geophys. Res. Planets 126. e2020JE006613.
Savage, P.S., Georg, R.B., Williams, H.M., Burton, K.W., Halliday, A.N., 2011. Silicon isotope fractionation during magmatic differentiation. Geochim. Cosmochim. Acta 75, 6124–6139.
Savage, P.S., Armytage, R.M.G., Georg, R.B., Halliday, A.N., 2014. High temperature silicon isotope geochemistry. Lithos 190–191, 500–519.
Savage, P.S., Moynier, F., 2013. Silicon isotopic variation in enstatite meteorites: Clues to their origin and Earth-forming material. Earth Planet. Sci. Lett. 361, 487–496.
Schaefer, L., Elkins-Tanton, L.T., 2018. Magma oceans as a critical stage in the tectonic development of rocky planets. Philos. Trans. R. Soc. Math. Phys. Eng. Sci. 376, 20180109.
Shahar, A., Ziegler, K., Young, E.D., Ricolleau, A., Schauble, E.A., Fei, Y., 2009. Experimentally determined Si isotope fractionation between silicate and Fe metal and implications for Earth's core formation. Earth Planet. Sci. Lett. 288, 228–234.
Shahar, A., Hillgren, V.J., Young, E.D., Fei, Y., Macris, C.A., Deng, L., 2011. High-temperature Si isotope fractionation between iron metal and silicate. Geochim. Cosmochim. Acta 75, 7688–7697.
Solomatov, V.S., 2000. Fluid Dynamics of a Terrestrial Magma Ocean. In: Canup, R., Righter, K. (Eds.), Origin of the Earth and Moon. Univ. of Arizona Press, Tucson, Arizona, pp. 323–338.
Solomatov, V.S., 2007. Magma Oceans and Primordial Mantle Differentiation. In: Treatise on Geophysics, pp. 91–119.
Solomatova, N.V., Caracas, R., 2019. Pressure-induced coordination changes in a pyrolitic silicate melt from ab initio molecular dynamics simulations. J. Geophys. Res. Solid Earth 124, 11232–11250.
Sossi, P.A., Nebel, O., Anand, M., Poitrasson, F., 2016. On the iron isotope composition of Mars and volatile depletion in the terrestrial planets. Earth Planet. Sci. Lett. 449, 360–371.
Stähler, S.C., Khan, A., Banerdt, W.B., Lognonné, P., Giardini, D., Ceylan, S., Drilleau, M., Duran, A.C., Garcia, R.F., Huang, Q., Kim, D., Lekic, V., Samuel, H., Schimmel, M., Schmerr, N., Sollberger, D., Stutzmann, É., Xu, Z., Antonangeli, D., Charalambous, C., Davis, P.M., Irving, J.C.E., Kawamura, T., Knapmeyer, M., Maguire, R., Marusiak, A.G., Panning, M.P., Perrin, C., Plesa, A.-C., Rivoldini, A., Schmelzbach, C., Zenhäusern, G., Beucler, É., Clinton, J., Dahmen, N., van Driel, M., Gudkova, T., Horleston, A., Pike, W.T., Plasman, M., Smrekar, S.E., 2021. Seismic detection of the martian core. Science 373, 443–448.
Steenstra, E.S., Seegers, A.X., Putter, R., Berndt, J., Klemme, S., Matveev, S., Bullock, E. S., van Westrenen, W., 2020. Metal-silicate partitioning systematics of siderophile elements at reducing conditions: A new experimental database. Icarus 335, 113391.
Stolper, E., McSween, H.Y., Hays, J.F., 1979. A petrogenetic model of the relationships among achondritic meteorites. Geochim. Cosmochim. Acta 43, 589–602.
Tang, H., Young, E.D., 2020. Evaporation from the lunar magma ocean was not the mechanism for fractionation of the Moon's moderately volatile elements. Planet. Sci. J. 1, 49.
Taylor, G.J., 2013. The bulk composition of Mars. Geochemistry 73, 401–420.
Terasaki, H., Rubie, D.C., Mann, U., Frost, D., Langenhorst, F., 2005. The effects of oxygen, sulphur and silicon on the dihedral angles between Fe-rich liquid metal and olivine, ringwoodite and silicate perovskite: implications for planetary core formation. Lunar and Planet. Sci. Conf XXXVI. 1129.
Treiman, A.H., Gleason, J.D., Bogard, D.D., 2000. The SNC meteorites are from Mars. Planet. Space Sci. 48, 1213–1230.
Udry, A., Balta, J.B., McSween, H.Y., 2014. Exploring fractionation models for Martian magmas. J. Geophys. Res. Planets 119, 1–18.
Udry, A., Howarth, G.H., Herd, C.D.K., Day, J.M.D., Lapen, T.J., Filiberto, J., 2020. What martian meteorites reveal about the interior and surface of Mars. J. Geophys. Res.: Planets 125, e2020JE006523.
Wadhwa, M., 2001. Redox state of Mars' upper mantle and crust from Eu Anomalies in shergottite pyroxenes. Science 291, 1527–1530.
Williams, H.M., Matthews, S., Rizo, H., Shorttle, O., 2021. Iron isotopes trace primordial magma ocean cumulates melting in Earth's upper mantle. Sci. Adv. 7, 11.
Yang, S., Humayun, M., Righter, K., Jefferson, G., Fields, D., Irving, A.J., 2015. Siderophile and chalcophile element abundances in shergottites: Implications for Martian core formation. Meteorit. Planet. Sci. 50, 691–714.
Yoshizaki, T., McDonough, W.F., 2020. The composition of Mars. Geochim. Cosmochim. Acta 273, 137–162.
Young, E.D., Shahar, A., Nimmo, F., Schlichting, H.E., Schauble, E.A., Tang, H., Labidi, J., 2019. Near-equilibrium isotope fractionation during planetesimal evaporation. Icarus 323, 1–15.
Zambardi, T., Poitrasson, F., 2011. Precise determination of dilicon isotopes in silicate Rock reference materials by MC-ICP-MS. Geostand. Geoanalytical Res. 35, 89–99.
Zambardi, T., Poitrasson, F., Corgne, A., Méheut, M., Quitté, G., Anand, M., 2013. Silicon isotope variations in the inner solar system: Implications for planetary formation, differentiation and composition. Geochim. Cosmochim. Acta 121, 67–83.